Journal of Engineering Mathematics **38:** 173–190, 2000.

Mathematical modelling of heat transfer during electron-beam autocrucible melting by means of the steady-state Stefan problem

YU. A. MITROPOLSKY, A. A. BEREZOVSKY and YU. V. ZHERNOVYI
Institute of Mathematics, National Academy of Sciences of Ukraine, Tereshchenkivska Str. 252601, Kyiv-4, Ukraine

Received 14 August 1997; accepted in revised form 23 August 1999

Abstract. A two-dimensional axisymmetric mathematical model of electron-beam autocrucible melting is developed and examined. Here, the hypothesis is used that forced convective heat transfer in the melt may be modelled with the help of the coefficient of effective thermal conductivity, λ_E. A simplified approach is used in which λ_E is assumed to be known. In another approach the value of λ_E depends on a prescribed value of a mean melt-stirring velocity and a mean liquid-pool radius which is determined in the course of solving of the problem. With the help of the Kirchoff transformation and a Green function we may reduce the problem to a nonlinear Hammerstein integral equation. Here, a dependence of the thermal-conductivity coefficient on the temperature, $\lambda_S(T)$, at the cooled surfaces is disregarded and constant (mean) values of λ_S are utilized. In order to solve the problem in the case where this dependence $\lambda_S(T)$ is taken into account, an axuiliary Green-function method is proposed which also permits to take into account a change of the heat-exchange coefficients on the autocrucible. This reduces the problem to a system of three integral Hammerstein equations. Numerical solutions of the nonlinear integral equations are obtained with the help of a variational (projective-net) method for the case of circular scanning of an electron beam over the heated surface. The computational results are well consistent with experimental data.

Key words: melting, electron beam, circular scanning, steady-state Stefan problem, auxiliary Green-function method.

1. Introduction

In order to produce refractory metals and alloys one applies vacuum electron-beam autocrucible melting (EBAM) [1, 2], which is a special casting method. The main advantage of this method (in comparison with other methods of electric metallurgy) is the high degree of metal refining from harmful nonmetallic and gas inclusions. Complexity of thermal, hydrodynamical and physicochemical processes in an autocrucible, high temperatures and profound vacuum not only considerably complicate experimental studies of temperature fields in a melted portion of material, but make such studies also, for some refractory metals, problematical. In this connection, besides experimental methods a decisive role is played by mathematical methods of computation and prediction of thermal and kinetic characteristics of the melting process.

EBAM is realized applying melt electromagnetic stirring (MEMS) over the whole volume of the liquid pool, enabling the increase of the end metal discharge. Complex mathematical models in the form of a set of differential equations of heat and mass transfer, which take account of hydrodynamic and electromagnetic processes, can be used for melting process modelling. Such models are extremely laborious and their numerical realization requires much computer time. In order to determine the basic technological parameters of the EBAM process on the basis of numerical calculations, it is advantageous to use simplified mathematical mod-

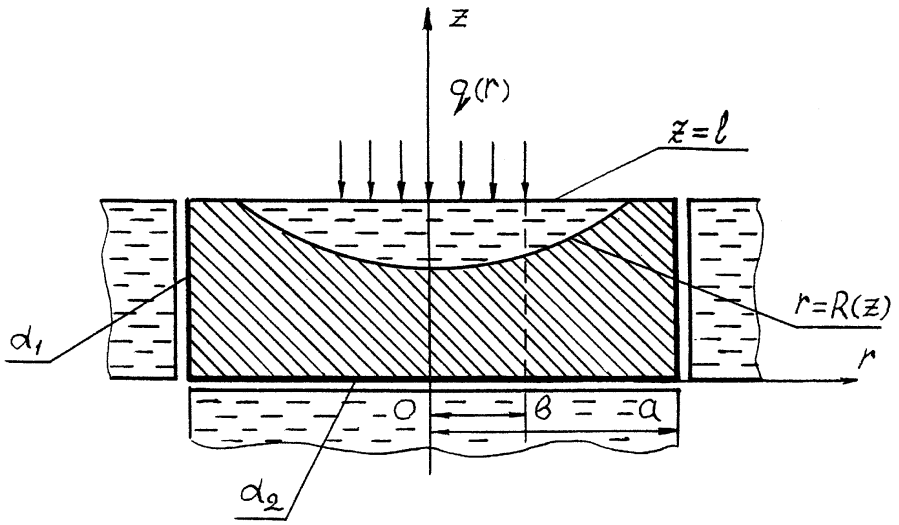

Figure 1. Scheme of the electron-beam autocrucible melting process in an autocrucible.

els [3–8], based on special statements of heat-conduction problems, including phase-change metal melt phenomena (Stefan problems). It is necessary to find the temperature fields in both solid and liquid metal, as well as its moving isothermal surface on which absorption of the melting heat takes place.

Solid-liquid phase-change problems occur in a diverse range of technical applications, such as metal processing, welding, environmental engineering and solar energy [9]. A few recent advances are discussed in [9] with special emphasis on the phase change of metals. An extensive review of moving and free-boundary problems related to the heat equation, particularly regarding the Stefan problem, can be found, for example, in [10].

Simplified mathematical models of heat transfer during electron-beam autocrucible melting are developed and examined in [8]. To obtain an approximate description of the liquid-pool dynamics, the one-dimensional Stefan problem for an 'equivalent' spherical shell is considered. The corresponding steady-state problem admits an exact analytical solution by means of which the dependence of the melt volume W, and melt overheating ΔT, on input data are obtained. Also, the basic melting parameters are determined ensuring that the preassigned W and ΔT are obtained. To solve the one-dimensional nonstationary Stefan problem by the variational method, it is essential that we use a construction of the exact solution of the steady-state Stefan problem. As a result, the problem is reduced to a Cauchy problem for a set of nonlinear ordinary differential equations. As far as the isotherm field is concerned, the obtained approximate solutions are reasonably consistent with numerical results obtained with the help of an implicit difference scheme for the Stefan problem.

In this paper we present a two-dimensional axisymmetric steady-state mathematical model which corresponds adequately to the thermophysical model of the EBAM.

2. Mathematical model

Let us describe the process under consideration and construct a mathematical model for it.

The autocrucible has a cylindrical form (Figure 1), its lateral surface ($r = a$) and bottom surface ($z = 0$) are cooled, and energy absorption of the electron-beam heating with a flux

density q occurs in the focal spot of radius $b < a$ on the surface $z = l$. The generated thermal energy is spent on metal heating, on melting heat, that can be represented by heat flows distributed along a melting isotherm (an interface between the solid and liquid phases) with a constant linear density. Besides, from the lateral and bottom surfaces, heat exchange with the surroundings (a water-cooled contour) occurs through conduction and radiation in a manner that is difficult to control. The heat losses through radiation and evaporation take place from the heated surface.

Heating is realized by a focused electron beam scanning over the heated surface. The level of the accelerating voltage of an electron gun determines the injection depth of electrons into the metal and defines the character of the heat source used for the modelling of the electron-beam heating. In most cases, electron guns of the axial type with accelerating voltages equal to 40–50 kV can be used [1]. Calculations by the Shonland formula [11] show that in this case the electron injection depth does not exceed 10^{-5} m into metal. Therefore, computation of the metal temperature by means of the mathematical model with a surface source of electron-beam heating, as used in this paper, assumes a relative error not exceeding 0·01% in comparison to the case which considers volume heat absorption.

When an electron beam scans over a circle, the center of which is situated on the axis $r = 0$, or when heating by means of a fixed electron beam is axisymmetric, the temperature field of an autocrucible is axisymmetric, $T = T(r, z)$. In accordance with the thermophysical meaning of the problem, there would be a stabilization to a limiting steady state if the overall supplied heat flux is completely balanced by means of the cooling system and by heat losses connected with radiation and evaporation. We may write the steady-state equations of heat conduction and the boundary conditions as follows

$$
\begin{aligned}
&\frac{1}{r}\frac{\partial}{\partial r}\left(r\lambda_S(T)\frac{\partial T}{\partial r}\right) + \frac{\partial}{\partial z}\left(\lambda_S(T)\frac{\partial T}{\partial z}\right) = 0, \quad (r, z) \in \Omega_S;\\
&\frac{1}{r}\frac{\partial}{\partial r}\left(r\lambda_L(T)\frac{\partial T}{\partial r}\right) + \frac{\partial}{\partial z}\left(\lambda_L(T)\frac{\partial T}{\partial z}\right) = 0, \quad (r, z) \in \Omega_L;\\
&\frac{\partial T}{\partial r} = 0, \quad r = 0; \qquad \lambda_S(T)\frac{\partial T}{\partial r} + \alpha_1(z)(T - T_W) = 0, \quad r = a;\\
&\lambda_S(T)\frac{\partial T}{\partial z} - \alpha_2(r)(T - T_W) = 0, \quad z = 0; \qquad \lambda(T)\frac{\partial T}{\partial z} = q(r) - f(T), \quad z = l.
\end{aligned}
\tag{1}
$$

Here the following notations are introduced:

$$
\lambda(T) = \begin{cases} \lambda_S(T), & T < T_m, \\ \lambda_L(T), & T \geqslant T_m, \end{cases}
$$

where T_W is the water temperature in the cooling system, T_m is the melting temperature, λ_L, λ_S are the thermal-conductivity coefficients for the liquid and solid phases, respectively; $q(r)$ is the electron-beam heating-power density being absorbed by the metal; $f(T) = \varepsilon\sigma T^4 + \eta(T - T_m)Q_{\mathrm{EV}}(T)$ is the flux density of heat losses at the expense of radiation and evaporation from the heated surface, $z = l$, ($\eta(T)$ is the Heavyside function). Further, ε, σ are the blackness degree and the Stefan-Boltzmann constant. In the general case the coefficients of heat exchange on the cooled surfaces, $\alpha_1(z), \alpha_2(r)$, may be functions of z, r, respectively. The domain $\Omega = \{(r, z) : 0 < r < a, 0 < z < l\}$ is divided by the solid-liquid boundary into

two subdomains $\Omega_S = \{(r, z) \in \Omega : T(r, z) < T_m\}$ and $\Omega_L = \{(r, z) \in \Omega : T(r, z) > T_m\}$, corresponding to the solid and liquid phases of the metal.

On an unknown solid-liquid interface, $r = R(z)$, the metal temperature and the melting temperature have to be equal and the same is true for the heat fluxes coming from the liquid and solid phases in the steady state, *i.e.*

$$T(R(z), z) = T_m, \qquad \lambda_L \frac{\partial T}{\partial n}\bigg|_{r=R(z)-0} = \lambda_S \frac{\partial T}{\partial n}\bigg|_{r=R(z)+0}. \tag{2}$$

We shall use the well-known hypothesis that forced convective heat transfer in melt conditioned by MEMS may be simulated with the help of the coefficient of effective thermal conductivity, $\lambda_E = \tilde{k}\lambda_L$, where λ_L is the coefficient of molecular thermal conductivity. To determine the value of $\tilde{k}$ we may use the formula obtained as a result of experimental investigations on turbulent heat transfer in the case of forced convection [12]:

$$\tilde{k} = \begin{cases} 0{\cdot}45(\mathrm{PrRe})^{0{\cdot}438}, & \text{if } \mathrm{PrRe} \leqslant 8600, \\ 1{\cdot}35 \times 10^{-6}(\mathrm{PrRe})^{1{\cdot}84}, & \text{if } \mathrm{PrRe} > 8600. \end{cases} \tag{3}$$

Taking into account that $\mathrm{PrRe} = 2v_m r_* C_{VL}/\lambda_L$, we see $\tilde{k}$ depends on the heat capacity of a unit of liquid-metal volume C_{VL} on a mean melt motion velocity v_m and on a mean pool radius r_*. In [1] the value $\tilde{k} = 10$ is used for calculating the case where electromagnetic stirring is sufficiently intense.

Assume the coefficient of effective thermal conductivity $\lambda_E = \text{const.}$ in the liquid phase domain, $\alpha_1(z) = \alpha_1 = \text{const.}$, we may transform the steady-state Stefan problem (1), (2) into the form

$$\begin{aligned}
&\frac{1}{r}\frac{\partial}{\partial r}\left(r\lambda_S(T)\frac{\partial T}{\partial r}\right) + \frac{\partial}{\partial z}\left(\lambda_S(T)\frac{\partial T}{\partial z}\right) = 0, \quad (r, z) \in \Omega_S; \\
&\frac{1}{r}\frac{\partial}{\partial r}\left(r\frac{\partial T}{\partial r}\right) + \frac{\partial^2 T}{\partial z^2} = 0, \quad (r, z) \in \Omega_L; \\
&\frac{\partial T}{\partial r} = 0, \quad r = 0; \qquad \lambda_S(T)\frac{\partial T}{\partial r} + \alpha_1(T - T_W) = 0, \quad r = a; \\
&\lambda_S(T)\frac{\partial T}{\partial z} - \alpha_2(T - T_W) = 0, \quad z = 0; \\
&\lambda(T)\frac{\partial T}{\partial r} = q(r) - f(T) = 0, \qquad z = l; \\
&T(R(z), z) = T_m, \qquad \lambda_E \frac{\partial T}{\partial n}\bigg|_{r=R(z)-0} = \lambda_S(T)\frac{\partial T}{\partial n}\bigg|_{r=R(z)+0}.
\end{aligned} \tag{4}$$

We shall represent the function $Q_{\mathrm{EV}}(T)$, designating the density of the heat flux of evaporation in the form $Q_{\mathrm{EV}}(T) = c_1 \exp(-c_2/T)$, where one may find the parameters c_1, c_2, using both data from experiment and the Clapeyron–Clausius law written for a thin gas layer closely approximating the evaporation surface, [13].

3. Procedure of solving of the Stefan problem

At present numerical methods for the Stefan problem, such as the finite-difference method and the finite-element method, are available [9, 10, 14–17]. However, realization of these methods in the case of two space dimensions is accompanied by considerable technical difficulties and insufficient economy of the computations. Therefore, we shall reduce the Stefan problem (4) to a nonlinear integral Hammerstein equation.

First we apply the Kirchhoff transformation of the function T

$$u(T) = \int_0^{T-T_W} \lambda(\tau)\,\mathrm{d}\tau.$$

If the dependence of the thermal-conductivity coefficient on the temperature is approximated by the step function

$$\lambda(T) = \lambda_i, \quad T_{i-1} \leqslant T \leqslant T_i, \qquad i = \overline{1, K}, \qquad (T_K = T_m, T_0 = T_W);$$
$$\lambda(T) = \tilde{k}\lambda_L, \quad T > T_m,$$

or by the linear dependence in the solid-phase domain

$$\lambda_S(T) = \lambda_S(T_0) - \beta(T - T_0), \quad T_0 \leqslant T \leqslant T_m, (T_0 = T_W);$$
$$\lambda(T) = \tilde{k}\lambda_L, \quad T > T_m,$$

we can find the inverse function $T(u)$ in analytical form.

If we exclude $T(r, z)$, from (4), we obtain a simpler boundary-value problem for a new unknown function, $u(r, z)$,

$$\begin{aligned}
&\frac{1}{r}\frac{\partial}{\partial r}\left(r\frac{\partial u}{\partial r}\right) + \frac{\partial^2 u}{\partial z^2} = 0, \quad 0 < r < a, \quad 0 < z < l,\\
&\frac{\partial u}{\partial r} = 0, \quad r = 0; \qquad \frac{\partial u}{\partial r} + h_1 u = 0, \quad r = a,\\
&\frac{\partial u}{\partial z} - h_2 u = 0, \quad z = 0; \qquad \frac{\partial u}{\partial z} = q(r) - f(T(u)), \quad z = l
\end{aligned} \tag{5}$$

and the condition for the determination of an interface $r = R(z)$ between the solid and liquid phases

$$u(R(z), z) = u_m. \tag{6}$$

Here $h_i = \alpha_i/\lambda_{Si}, i = 1, 2$, where λ_{Si} are mean values of λ_S on the surfaces $r = a$ and $z = 0$, respectively; $u_m = u(T_m)$.

We shall consider the Green function, $G(r, z; \rho, \eta)$, which is determined as a solution of the linear boundary-value problem with homogeneous boundary conditions

$$\frac{1}{r}\frac{\partial}{\partial r}\left(r\frac{\partial G}{\partial r}\right) + \frac{\partial^2 G}{\partial z^2} = -\delta(r - \rho)\delta(z - \eta), \quad 0 < r, \rho < a, \quad 0 < z, \eta < l,$$

$$\frac{\partial G(0,z;\rho,\eta)}{\partial r}=0, \qquad \frac{\partial G(a,z;\rho,\eta)}{\partial r}+h_1G(a,z;\rho,\eta)=0,$$
$$\frac{\partial G(r,0;\rho,\eta)}{\partial z}-h_2G(r,0;\rho,\eta)=0; \qquad \frac{\partial G(r,l;\rho,\eta)}{\partial z}=0,$$

where the formal relations for the Dirac function are given by

$$\int_0^l g_1(z)\delta(z-\eta)\,\mathrm{d}z=g_1(\eta), \qquad \int_0^a g_2(r)\delta(r-\rho)r\mathrm{d}r=g_2(\rho).$$

The Green function is found in the form

$$G(r,\rho;z,\eta)=\frac{2}{a^2}\sum_{n=1}^{\infty}\frac{\gamma_nJ_0(\gamma_n\rho)J_0(\gamma_nr)g_n(z,\eta)}{(h_1^2+\gamma_n^2)[\gamma_n\sinh(\gamma_nl)+h_2\cosh(\gamma_nl)]J_0^2(\gamma_na)},$$

where $g_n(z,\eta)=[\gamma_n\cosh(\gamma_n,z)+h_2\sinh(\gamma_n,z)]\cosh(\gamma_n(l-\eta))$, $z\leqslant\eta$; $g_n(\eta,z)=g_n(z,\eta)$; $\gamma_n>0$ are roots of the equation $h_1J_0(\gamma a)-\gamma J_1(\gamma a)=0$; $J_n(z)$ is the Bessel function of the first kind and nth order.

By means of the second Green formula probem (5) may be reduced to an equivalent nonlinear integral equation

$$u(r,z)=u_0(r,z)-\int_0^a G(r,z;\rho,l)f[T(u(\rho,l))]\rho\mathrm{d}\rho, \tag{7}$$

where

$$u_0(r,z)=\int_0^a q(\rho)G(r,z;\rho,l)\rho\mathrm{d}\rho.$$

Substituting $z=l$ in (7), we arrive at the nonlinear Hammerstein integral equation for the function $v(r)=u(r,l)$

$$v(r)=v_0(r)-\int_0^a G(r,\rho)f[T(v(\rho))]\rho\mathrm{d}\rho, \tag{8}$$

where $v_0(r)=u_0(r,l)$, $G(r,\rho)=G(r,l;\rho,l)$. Upon solving integral equation (8), we may find the function $u(r,z)$ and the solid-liquid interface $r=R(z)$ from quadrature (7) and Equation (6), respectively.

To find an approximate solution of Equation (8), we approximate $v(r)$ by the step function and define a mean integral value of $v(r)$ on the interval (r_{i-1},r_i) by v_i, where r_i are decomposition points of the segment $[0,a]$ which has been divided into M parts. After applying a variational method, we obtain a system of nonlinear equations for v_j, $j=\overline{1,M}$,

$$v_j=v_{0j}-\sum_{i=1}^{M}G_{ij}f(T(v_i)), \quad j=\overline{1,M}, \tag{9}$$

where the constants $v_{0,j}$, G_{ij} are found by integration of known functions.

Having determined v_j, $j = \overline{1, M}$, we can represent the modified temperature in the form of a series

$$u(r, z) = \frac{2}{a^2} \sum_{n=1}^{\infty} A_n(z) J_0(\gamma_n r), \tag{10}$$

where

$$A_n(z) = \left[\frac{\gamma_n}{4P_n} \int_0^a rq(r) J_0(\gamma_n r)\, \mathrm{d}r - \sum_{i=1}^{M} f(T(v_i)) A_{ni} \right] g_n(z);$$

$$A_{ni} = \frac{[r_i J_1(\gamma_n r_i) - r_{i-1} r J_1(\gamma_n r_{i-1})]}{P_n},$$

$$P_n = (\gamma_n^2 + h_1^2)[\gamma_n + h_2 - (\gamma_n - h_2)\ \exp(-2\gamma_n l)] J_0^2(\gamma_n a),$$

$$g_n(z) = (\gamma_n + h_2)\ \exp(-\gamma_n(l - z)) + (\gamma_n - h_2)\ \exp(-\gamma_n(l + z)).$$

Using a simplified approach, we can assume the coefficient of effective thermal conductivity to be known ($\lambda_E = \text{const.}$), independent of a solution of the heat-conduction problem. In that case system (9) remains to be solved.

Using another approach where a value of $\lambda_E = \tilde{k}\lambda_I$ is determined in the course of solving the problem, we can use formula (3) in accordance to which $\tilde{k}$ depends on a mean melt-stirring velocity v_m and a mean radius of the liquid pool, r_*. We shall assume that the value of v_m is determined by the action intensity of the MEMS system only. If the value of v_m is given, we may reduce the determination of $\tilde{k}$ to finding a mean integral value of the liquid pool radius

$$r_* = \frac{1}{l - z_0} \int_{z_0}^{l} R(z)\mathrm{d}z \tag{11}$$

over its depth, $H = l - z_0$, also to be determined. Here z_0 is a solution of the equation $R(z) = 0$. In this case it is impossible to find a solution of system (9) since the parameter $\tilde{k}$ is used for determining of a relation between the functions T and u.

Let us describe the solution procedure of the problem in this case. Evidently, we can find $\tilde{k} = \tilde{k}(r_*)$ from (3) and compute $\lambda_E = \tilde{k}(r_*)\lambda_L$ for every value of $r_* \in (0, a)$ and then we can solve system (9). Further, considering Equation (6) for a sequence of discrete values of z_i we can find a sequence of corresponding values of the function $r_i = R(z_i)$ by which we can compute the right side of equality (11). Thus, relation (11) can be written in the form

$$r_* = F(r_*), \tag{12}$$

where $F(r_*)$, is a function which for every $r_* \in (0, a)$ correlates to a computation result of the right side of (11) obtained in the way stated above. Thus, the determination of a mean integral value of the pool radius r_* is practically reduced to the numerical solution of the functional equation (12) by an iterative procedure.

Therefore, after finding an approximate solution of Equation (12), we can find a coefficient of the effective thermal conductivity $\lambda_E = \tilde{k}(r_*)\lambda_L$, a modified temperature field $u(r, z)$ and a solid-liquid boundary $r = R(z)$ with a mean integral value of the radius which is equal to r_*.

The desired steady-state temperature field $T(r, z)$ is determined by inversion of the Kirchhoff transformation $u(T)$.

The liquid-pool volume W, the mean integral melt overheating over the whole pool volume ΔT and the melt overheating on the pool surface ΔT_i are computed by means of the formulas

$$W = \pi \cdot \int_{z_0}^{l} R^2(z)\mathrm{d}z, \qquad \Delta T = \frac{2\pi}{W} \int_{z_0}^{l} \int_{0}^{R(z)} T(r, z) r \mathrm{d}r \mathrm{d}z - T_m,$$

$$\Delta T_l = \frac{2}{R^2(l)} \int_{0}^{R(l)} T(r, l) r \mathrm{d}r - T_m.$$

4. Determination of $q(r)$ in the case of circular electron-beam scanning

In practice, EBAM heating is realized by a focused electron beam scanning over the heated surface in accordance with a given program (a circle, a spiral, intersecting lines and others). Let us determine $q(r)$, a steady-state power-density distribution on the heated surface in the case of the scanning of an electron beam over a circle of radius $0 < R < a$. Let O_1 be the focal point of a beam situated in the plane $z = l$ and $|O O_1| = R$, where O is situated in the same plane on the autocrucible axis. Let us consider a point $M(\beta)$ at a distance r to the point O and one at a distance $y(\beta)$ to the point O_1, where $\beta =< O_1 O M(\beta)$. At $M(\beta)$ the value of the power density is equal to $q_0 \exp[-k_r y^2(\beta)]$, where $y^2(\beta) = R^2 + r^2 - 2rR \cos\beta$, $0 \leqslant \beta \leqslant \pi$ (from the cosine theorem); $q_0 = Pk_r/\pi$ is the value of the heating-power density at the focal point of a beam, P is the heating power being absorbed by the metal, $k_r = 2b^{-2}$ is a concentration coefficient of the heat source in the radial direction and b is a focal-spot radius. The density of the energy being absorbed at every point at a distances r from the point O and at the time when the electron beam traverses one full circle of radius R (in the rotation period $T_{\mathrm{sc}} = 2\pi R/v_{\mathrm{sc}}$, where v_{sc} is a scan velocity) is determined by the integral

$$\begin{aligned} E(r) &= 2q_0 \int_0^{T_{\mathrm{sc}}/2} \exp\{-k_r[r^2 + R^2 - 2Rr \cdot \cos(v_{\mathrm{sc}} t/R)]\}\, \mathrm{d}t \\ &= \frac{2Rq_0}{v_{\mathrm{sc}}} \exp[-k_r(r^2 + R^2)] \int_0^{\pi} \exp(2k_r r R \cdot \cos\beta)\mathrm{d}\beta. \end{aligned}$$

The function $q(r)$ is assumed to be the mean value of the energy density being absorbed per unit time

$$q(r) = \frac{E(r)}{T_{\mathrm{sc}}} = \frac{q_0}{\pi} \exp[-k_r(r^2 + R^2)] \int_0^{\pi} \exp(2k_r r R \cdot \cos\beta)\mathrm{d}\beta. \tag{13}$$

From (13) we obtain for $R = 0$ the known formula for the normal distribution $q(r)$ for the case of axisymmetric heating by a fixed beam: $q(r) = \exp(-k_r r^2)$. Expanding the exponential function under the integral sign in (13) as a Taylor series, we may write the expression for $q(r)$ as

$$q(r) = q_0 \exp[-k_r(r^2 + R^2)] \left[1 + \sum_{n=1}^{\infty} \frac{(2n-1)!!}{(2n)!!} \frac{(2k_r r R)^{2n}}{(2n)!} \right].$$

The investigation of the function $q(r)$ from (13) shows that a maximum point of $q(r)$, $r = r_0$, is determined by the equation

$$\int_0^{\pi} (R\cdot\cos\beta - r)\,\exp(2k_r r R\cdot\cos\beta)\mathrm{d}\beta = 0, \tag{14}$$

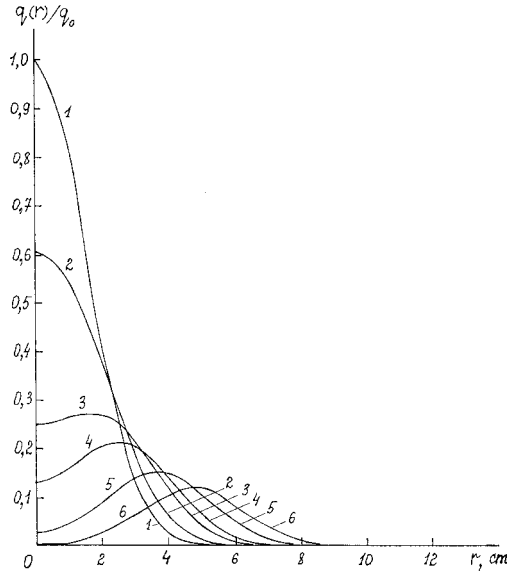

Figure 2. Relative power density distribution of an electron-beam over the heated surface for $b = 0{\cdot}03$ m and various values of circular scan radius: 1: $R = 0$ m; 2: $R = 0{\cdot}015$ m; 3: $= 0{\cdot}025$ m; 4: $R = 0{\cdot}03$ m; 5: $R = 0{\cdot}04$ m; 6: $R = 0{\cdot}4$ m.

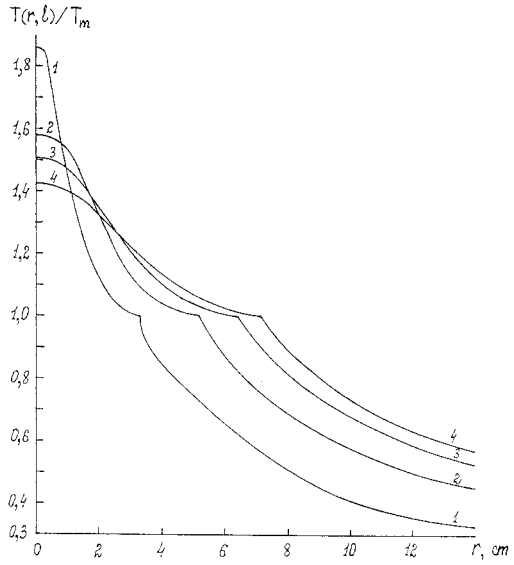

Figure 3. Influence of focal-spot radius on Niobium dimensionless temperature distribution over heated surface for $R = 0$ m; 1: $b = 0{\cdot}01$ m; 2: $b = 0{\cdot}02$ m; 3: $b = 0{\cdot}03$ m; 4: $b = 0{\cdot}04$ m.

from which we obtain the inequalities $0 \leqslant r_0 \leqslant R$. These inequalities are verified by a form of the curves $q(r)/q_0$ shown in Figure 2 for the case where $b = 0{\cdot}03$ m and the scan radius R takes various values: if $R = 0$ and $R = 0{\cdot}15$ m, then the maximum is at $r_0 = 0$, but if R is further increased, then the maximum points are situated on the interval $(0, R)$. Thus, for specific values of R, the trajectory (a circle) of a maximum absorption of the heating energy is situated inside the circle as bounded by the scan trajectory $r = R$, but not on the line $r = R$ of the focusing beam. We may write Equation (14) as

$$1 + \sum_{n=1}^{\infty} \frac{(2n-1)!!}{(2n)!}\left[\frac{2k_r r^2}{(2n)!} - \frac{1}{(2n-1)!}\right](2k_r)^{2n-1}R^{2n}r^{2n-2} = 0.$$

Restricting ourselves to two terms of the series, we obtain the biquadratic equation

$$k_r^4 R^4 r^4 + 2k_r^2 R^2(2 - k_r R^2)r^2 - 4(k_r R^2 - 1) = 0,$$

from which we find the following approximate value of r_0

$$r_0 \approx \frac{\sqrt{2(k_r R^2 - 1)}}{k_r R}$$

and from the condition $r_0 > 0$ we have

$$R > \frac{1}{\sqrt{k_r}} = \frac{b}{\sqrt{2}}.$$

5. Numerical results

To illustrate the mathematical model developed in this paper, we did calculations of steady-state EBAM heat regimes for niobium in an autocrucible of diameter 280 mm ($a = 0{\cdot}14$ m), where a level of the metal in the autocrucible was $l = 0{\cdot}14$ m and the electron-beam power was $P_0 = 190$ kW. In accordance with [1] the electron-beam heating efficiency is equal to $\eta = 0{\cdot}7$; therefore, we assume that the power being absorbed by the metal is equal to $P = \eta P_0 = 133$ kW.

For the calculations we take the following values of the parameters [1, 18]: $T_m = 2740$ K; $C_{VL} = 0{\cdot}2772 \times 10^7$ J/(m^{3}K); $T_W = 300$ K; $\lambda_L = 56{\cdot}2716$ W/(m·K); $\alpha_1 = \alpha_2 = 400$ W/(m^{2}K); $\varepsilon = 0{\cdot}4$; $c_1 = 0{\cdot}31102 \times 10^{18}$; $c_2 = 93868{\cdot}526$ (the values of c_1 and c_2 were obtained on the basis of the experimental data from [3]). In the solid-phase domain we consider a step dependence of the thermal-conductivity coefficient on the temperature obtained with the help of data for the niobium heat conductivity [18]. We consider axisymmetric heating of metal by a fixed ($R = 0$) or scanning electron beam over a circle of radius $0 < R < a$, where a steady-state distribution of the power density $q(r)$ on the heating surface is determined as in (13).

In Figures 3 and 4 the curves of the metal-temperature distribution over the heated surface, as obtained for various values of the scan radius R($R = 0$ for Figure 3) and the focal-spot radius b, provided that the MEMS system is used, are shown. Here we take $v_m = 0{\cdot}3$ m/s because in autocrucibles that have been subjected frequently to MEMS systems, the metal velocity is known to be close to this value (see [1]). The values of $\tilde{k}$ obtained for values of the scan radius between 0 to 6 cm range from 8·34 to 13·11 when $b = 0{\cdot}01$ m and from 11·79 to 12·88 for $b = 0{\cdot}04$ m, that is, these values are close to $\tilde{k} = 10$[1]. A comparison of the curves of the melt-surface temperature obtained for $b = 0{\cdot}03$ m, $v_m = 0{\cdot}3$ m/s (continuous lines) and $\tilde{k} = 10$ (dashed) is presented in Figure 5.

The temperature curves $T(r, l)$ for different values of R reproduce the behavior of the corresponding dependences on $q(r)$ (Figure 2). Increasing the scan radius and the focal-spot radius lead to a more uniform distribution of the density of the energy that is absorbed over the heating surface and consequently, a decrease of the temperature gradient as well as natural increase of the pool radius on the surface $z = l$. If R is increased, the points of maximum temperature attainment recede from the center $r = 0$ of the pool surface, the temperature $T(0, l)$ decreases and approaches the melting temperature T_m. Therefore, if the scan radius increases considerably ($R > 0{\cdot}06$ m) the formation of a solid metal zone in the central part of the pool is possible. Above the melting temperature, the temperature curves have a break point. This is stipulated by the difference of the thermal-conductivity coefficients for the melt and solid metal.

To determine the error made when the nonlinear boundary-value problem (5) is solved approximately, we have computed the value of the total energy losses from the surface $z = l$, $z = 0$ and $r = a$ which, for the exact solution of the steady-state problem, must be equal to the value of the power P absorbed by the metal. Calculations carried out with the use of

the niobium data and the parameters stated above for $b = 0{\cdot}03$ m show that the error made during the process of determining the temperature on the surfaces $z = l, z = 0$ and $r = a$, and computed with respect to the value of the power absorbed, is equal to 1·36% for $R = 0$ and to 0·165% for $R = 0{\cdot}03$ m.

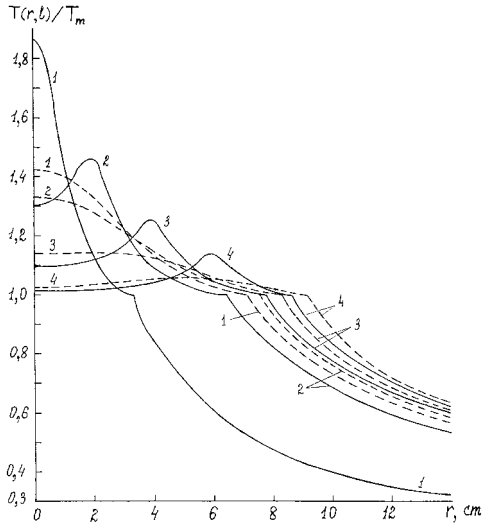

Figure 4. Influence of circular scan radius on Niobium dimensionless temperature distribution over heating surface for $b = 0{\cdot}01$ m (continuous lines) and $b = 0{\cdot}04$ m (dahsed). 1: $R = 0$ m; 2: $R = 0{\cdot}02$ m; 3: $R = 0{\cdot}04$ m; 4: $R = 0{\cdot}06$ m.

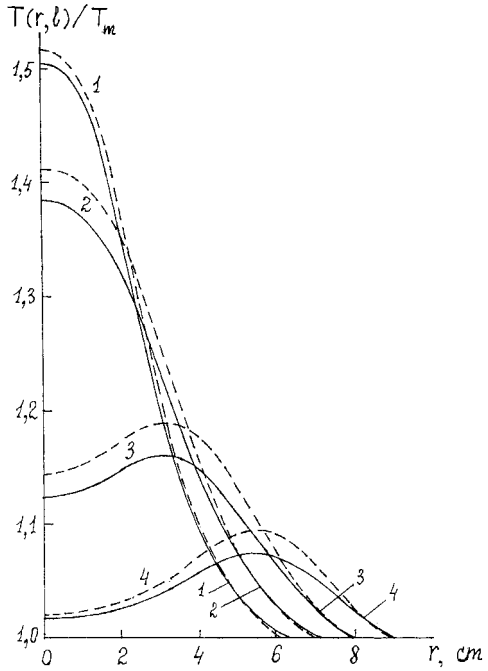

Figure 5. Comparison of Niobium dimensionless temperature distributions over heated surface for $b = 0{\cdot}03$ m, $v_m = 0{\cdot}03$ m/s (continuous lines) and $\tilde{k} = 10$ (dashed) for various values of scan radius. 1: $R = 0$ m; 2: $R = 0{\cdot}02$ m; 3: $R = 0{\cdot}04$ m; 4: $R = 0{\cdot}06$ m.

Figure 6 shows the sections of the solid-liquid interfaces, $r = R(z)$, that were obtained for various values of the scan radius R for the cases where the MEMS system is used ($v_m = 0{\cdot}3$ m/s), including the case when then the radiation and evaporation heat losses from the surface $z = l$ are disregarded ($f = 0$) and for the case where forced melt stirring is omitted ($v_m = 0{\cdot}005$ m/s). In this last case the value of $\tilde{k}$ changes from 1·44 to 2·00. When the scan radius R is varried from 0 to 0·05 m. The pool depth increases with R and reaches a maximum for a specific value of the scan radius, but it decreases when R is further increased. At the expense of heat losses from the heated surface, the depth and the radius of the pool decrease approximately by half. In the case of melting, when MEMS is used, the pool reaches its greatest diameter not on the surface $z = l$, but a little below it; thus, the solid-liquid interface has a small bend in the direction of the axis $r = 0$, giving the pool an ellipsoidal form as observed in practice. The presence of this bend is explained as follows: the heat losses exceed the energy absorbed in the points where the melting isotherm surface intersects the surface $z = l$; therefore, the derivative of the temperature with respect to the axial coordinate, z, is negative close to the surface $z = l$. In the two other cases this derivative is positive ($v_m = 0{\cdot}005$ m/s) and in another is equal to zero ($f = 0$). It should be noted that, for the linear problem ($f = 0$), the position of the solid-liquid phase boundary $r = R(z)$ becomes independent of the effective thermal-conductivity coefficient.

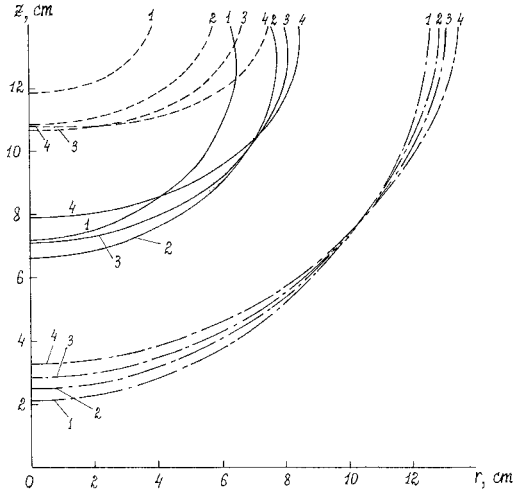

Figure 6. Influence of the value of circular scan radius on sections of solid-liquid interfaces $r = R(z)$, obtained at $b = 0{\cdot}03$ m for the cases where $v_m = 0{\cdot}3$ m/s (continuous lines), $v_m = 0{\cdot}005$ m/s (dashed) and $f = 0$ (dot-and-dash). 1: $R = 0$ m; 2: $R = 0{\cdot}03$ m; 3: $R = 0{\cdot}04$ m; 4: $R = 0{\cdot}05$ m.

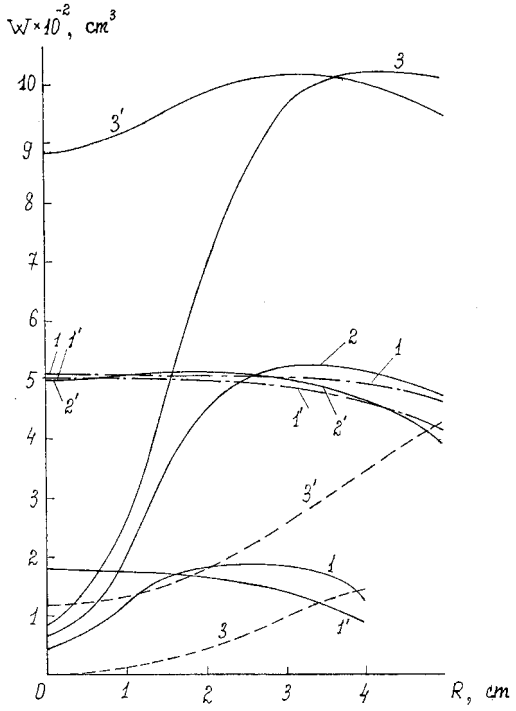

Figure 7. Dependences of niobium liquid pool volume on scan radius for the cases where $v_m = 0{\cdot}3$ m/s (continuous lines), $v_m = 0{\cdot}005$ m/s (dashed) and $f = 0$ (dot-and-dash) for $b = 0{\cdot}01$ m (indexing 1–3) and $b = 0{\cdot}04$ m ($1'$–$3'$) and various values of power $P{\cdot}1, 1'$: $P = 65$ kW; $2, 2'$: $P = 100$ kW; $3, 3'$: $P = 133$ kW.

The graphs presented in Figures 7 and 8 show that an increase of the scan radius causes an increase of the pool volume and a decrease of the melt overheating. This is fully explained by the observation that the energy absorption is distributed more uniformly over the heated surface when R is increased. But in the case of melting with MEMS an extreme increase of the scan radius causes a decrease of the volume, and for every b the function $W(R)$ has a maximum at some point. A comparison of the curves $W(R)$ obtained for $v_m = 0{\cdot}005$ m/s and $v_m = 0{\cdot}3$ m/s shows that the use of MEMS permits to obtain for $R = 0$ a volume which is 7·5–20 times bigger (depending on the value of b) and for $R = 5$ cm, for example, 2·8–3·5 times bigger. Applying a circular scan of the electron beam, one can make the pool volume twelve times bigger for $b = 1$ cm (in comparison with the axisymmetric heating by a fixed beam) and for $b = 4$ cm the volume is increased by 15%. At the expense of heat losses from the heated surface the liquid pool volume is decreased by a facts of 2·5–4 for absorbed-power levels in the range $P = 65$–133 kW. The melt overheating on the pool surface is more than two times bigger than the mean integral overheating over the whole pool volume (Figure 8).

In Figure 9 we show the dependence of the relative total energy losses by radiation and evaporation from the heated surface, $P_{\mathrm{RD+EV}}/P$, (continuous lines), the relative losses by radiation, P_{RD}/P, (dashed lines) and by metal evaporation, P_{EV}/P, (dot-and-dash ones) on the scan radius R for $\tilde{k} = 10$ and various values of the focal-spot radius. This analysis allows us to conclude that an increase of the scan radius will lead to lower total losses $P_{\mathrm{RD+EV}}$;

the contribution of the radiation losses is increased and evaporation is decreased. Let us pay attention to the fact that the total losses are stabilised and the presence of a minimum value of $P_{\mathrm{RD+EV}}/P$ for a specific value of the scan radius (to which a maximum value of the liquid pool volume corresponds (Figure 7)). This points to the possibility that the EBAM technological process can be constructed in such a way that energy losses through radiation and evaporation can be reduced to a minimum.

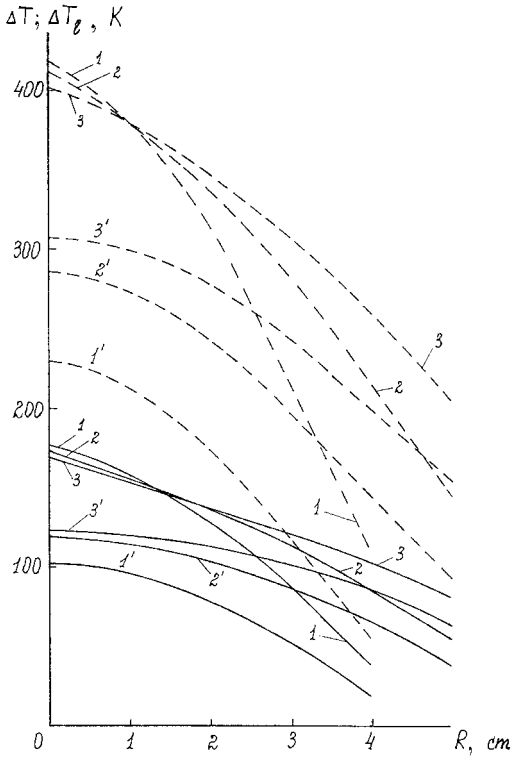

Figure 8. Dependences of niobium mean integral overheating over the whole pool volume (continuous lines) and melt overheating on pool surface (dashed) on scan radius for the cases where $b = 0{\cdot}01$ m (indexing 1–3) and $b = 0{\cdot}04$ m (1′–3′) for various values of power $P{\cdot}1, 1'$: $P = 65$ kW; $2, 2'$: $P = 100$ kW; $3, 3'$: $P = 133$ kW.

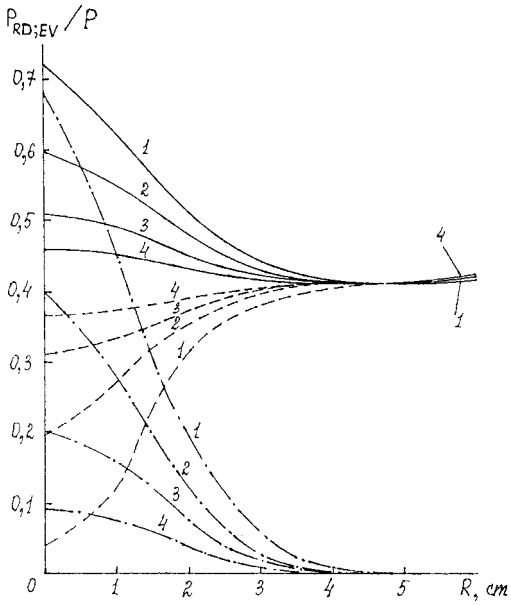

Figure 9. Dependences of relative energy losses from the heating surface (continuous lines), losses at the expense of radiation (dashed) and metal evaporation (dot-and-dash) on scan radius for $\tilde{k} = 10$ and various values of the focal spot radius. 1: $b = 0{\cdot}01$ m; 2: $b = 0{\cdot}02$ m; 3: $b = 0{\cdot}03$ m; 4: $b = 0{\cdot}04$ m.

6. Auxiliary Green function

In the reduction of the Stefan problem (4) to problem (5) for the modified temperature $u(r, z)$ a dependence of the thermal-conductivity coefficient $\lambda_S(T)$ on temperature on the surfaces $r = a$ and $z = 0$ was not taken into account; instead constant (mean) values of λ_S were utilized. After applying the Kirchhoff transformation to the more complicated problem (1), (2), we now obtain a nonlinear boundary-value problem for $u(r, z)$

$$\begin{aligned}
&\frac{1}{r}\frac{\partial}{\partial r}\left(r\frac{\partial u}{\partial r}\right)+\frac{\partial^2 u}{\partial z^2}=0, \quad 0<r<a, \ \ 0<z<l;\\
&\frac{\partial u}{\partial r}=0, \quad r=0; \qquad \frac{\partial u}{\partial r}+\alpha_1(z)[T(u)-T_W]=0, \quad r=a;\\
&\frac{\partial u}{\partial z}-\alpha_2(r)[T(u)-T_W]=0, \quad z=0; \qquad \frac{\partial u}{\partial z}=q(r)-f(T(u)), \quad z=l.
\end{aligned} \tag{15}$$

Because a Green's function for the linear boundary-value problem corresponding to problem (15) does not exist, we represent the boundary condition on the surface $r = a$ in the form

$$\frac{\partial u}{\partial r}+hu=hu-\alpha_1(z)[T(u)-T_W], \quad r=a, \quad 0<z<l,$$

(h is an arbitrary number such that $0 < h < \infty$) and formulate the boundary-value problem for an auxiliary Green function $G_a(r, z; \rho, x)$

$$\frac{1}{r}\frac{\partial}{\partial r}\left(r\frac{\partial G_a}{\partial r}\right)+\frac{\partial^2 G_a}{\partial z^2}=-\delta(r-\rho)\delta(z-x), \quad 0<r,\ \rho<a, \quad 0<z,\ x<l,$$

$$\frac{\partial G_a(0,z;\rho,x)}{\partial r}=0, \qquad \frac{\partial G_a(a,z;\rho,x)}{\partial r}+hG_a(a,z;\rho,x)=0,$$

$$\frac{\partial G_a(r,0;\rho,x)}{\partial z}=0, \qquad \frac{\partial G_a(r,l;\rho,x)}{\partial z}=0.$$

The solution may be written in the form

$$G_a(r,z;\rho,x)=\frac{1}{a^2}\sum_{n=1}^{\infty}\frac{G_n(x,z)}{P_n}J_0(\gamma_n\rho)J_0(\gamma_n r),$$

$$G_n(x,z)=\gamma_n\ \exp[-\gamma_n(z-x)][1+\exp(-2\gamma_n x)][1+\exp(-2\gamma_n(l-z))], \quad x\leqslant z,$$

$$G_n(x,z)=G_n(z,x), \qquad P_n=(\gamma_n^2+h^2)[1-\exp(-2\gamma_n l)]J_0^2(\gamma_n a),$$

where $0 < \gamma_1 < \gamma_2 < \gamma_3 < \cdots$ are the roots of the equation $hJ_0(\gamma a) - \gamma J_1(\gamma a) = 0$.

This auxiliary Green-function method was proposed first in [19].

Introducing the following notations: $u(r, 0) = v_0(r)$, $u(r, l) = v_1(r)$, $u(a, z) = w(z)$, and using the second Green formula, we can express the unknown function $u(r, z)$ in terms of its values on the surfaces $z = 0$, $z = l$ and $r = a$:

$$\begin{aligned}
u(r,z) \ = \ &\int_0^a G_a(r,z;\rho,l)[q(\rho)-f(T(v_1(\rho)))]\rho\mathrm{d}\rho\\
&+a\int_0^l G_a(r,z;a,x)\{hw(x)-\alpha_1(x)[T(w(x))-T_w\}\mathrm{d}x\\
&-\int_0^a G_a(r,z;\rho,0)\alpha_2(\rho)[T(v_0(\rho))-T_W]\rho\mathrm{d}\rho.
\end{aligned} \tag{16}$$

Writing the integral relation (16) for $z = 0$, $z = l$ and $r = a$ consecutively, we obtain a system of three Hammerstein integral equations for the functions $v_0(r)$, $v_1(r)$ and $w(z)$. Upon solving this system approximately by means of a projective-net method, we may find $u(r, z)$ from (16).

The numerical solution of the system of integral equations obtained from (16), is found for the case of a steady-state temperature regime for the EBAM of niobium in an autocrucible of diameter 280 mm ($a = 0{\cdot}14$ m) with a metal level equal to $l = 0{\cdot}14$ m. We have assumed that $\alpha_2(r) \equiv 0$, $R = 0$, $b = 0{\cdot}04$ m, $\lambda_E = 562{\cdot}716$ W/(m·K). We have considered a linear dependence of the thermal-conductivity coefficient $\lambda_S(T)$ on the temperature based on the niobium thermal-conductivity data [18]: $\lambda_S(T) = \lambda_0 + \beta(T - T_W)$, $\lambda_0 = 53{\cdot}7$ W/(m·K), $\beta = 0{\cdot}01063$, $T_W = 300$ K.

Figure 10 presents the sections of the solid-liquid interfaces $r = R(z)$ obtained for $\alpha_1 = 400$ W/(m^{2}K) and for two values of the electron-beam heating power absorbed by the metal, $P = 130$ kW and $P = 65$ kW, and for various representations of the thermal-conductivity coefficient in the solid-phase domain: $\lambda_S = 54{\cdot}1$ W/(m·K) (the value from [1]), $\lambda_S = 66{\cdot}2$ W/(m·K) (a mean value in the temperature interval from 300 K to 2740 K) as well as a linear dependence $\lambda_S = \lambda_S(T)$ (curve 3). Curves 4 and 5 correspond to the case where $\lambda_S = \lambda_S(T)$ and a linear dependence of the heat exchange coefficient $\alpha_1(z)$ on z is assumed. Here, $\alpha_1(0) = 300$, $\alpha_1(l) = 500$ W/(m^{2}K) (the curve 4); curve 5 corresponds to the values $\alpha_1(0) = 200$, $\alpha_1(l) = 600$ W/(m^{2}K).

Thus, since the dependence of the thermal conductivity on temperature could be taken into account, thanks to the introduction of the auxiliary Green-function method for the example in question, the refinement of the result for the melt volume ranges from 10·9% (comparison of the curves 2 and 3) to 36·6% (comparison of the curves 1 and 3). Besides, the application of the auxiliary Green-function method permits to take into account a change of the heat-exchange coefficients on the cooled surfaces, of the autocrucible which, in turn, for the preceding example leads to a refinement of the results of the calculation of the melt volume by 5·7% (a comparison of the curves 3 and 4) and by 10·2% (comparison of the curves 3 and 5).

If we compare the obtained values of the liquid-pool volume and the results obtained for the constant value $\lambda_S = 66{\cdot}2$ W/(m·K) on surface $r = a$ and a step dependence $\lambda_S = \lambda_S(T)$ in the solid-phase domain Ω_S, we see that such assumptions lead to an enlargement of the volume for $\alpha_1 = 400$ W/(m^{2}K), $P = 130$ kW by 15·3% and by 9·8% for $P = 65$ kW. In addition, the maximum rise of the metal temperature in the solid-phase domain for $P = 130\,kW$ is 100 K and 40 K at the center of the focal spot on the heated surface.

7. Comparison with experimental data

To verify the agreement of the mathematical model described by the Stefan problem (4) to real thermal EBAM regimes, we have carried out a comparison of the computational results with known experimental data given in [1]. For the experimental case of niobium melting in an autocrucible of diameter 280 mm with MEMS for an electron beam of maximum power $P_0 = 190$ kW, the mass of the obtained melt oscillates from 8·4 kg to 8·7 kg, that is, its volume varies between 976·7 cm^3 and 1011·6 cm^3. In Figure 7 the curves $W(R)$, corresponding to the value $P = 133$ kW, intersect this band of values for scan radius values between 3 and 5 cm.

In accordance with [1] in the case of EBAM without forced stirring the pool depth of zirconium in an autocrucible of diameter 250 mm amounts to 24–28 mm. In accordance with our

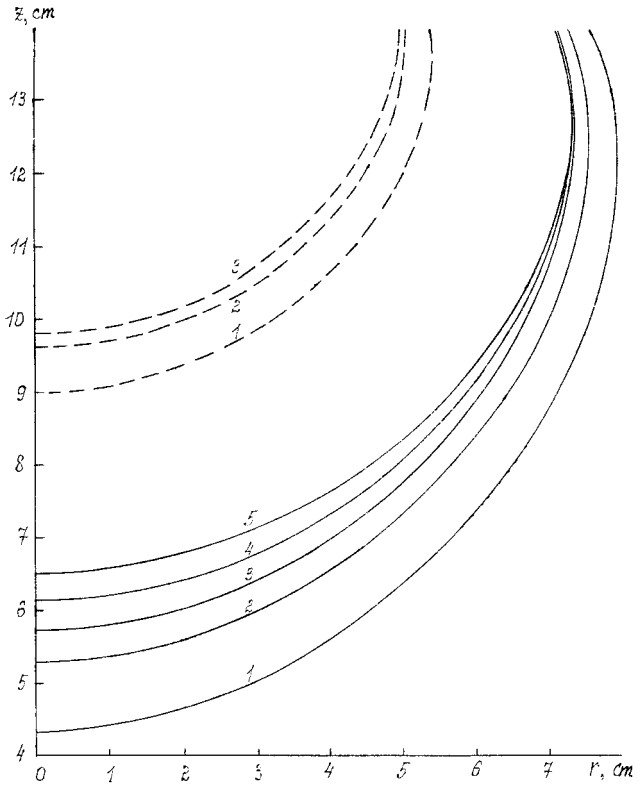

Figure 10. Sections of solid-liquid interfaces $r = R(z)$ obtained for the cases where $P = 130\,\text{kW}$ (continuous lines) and $P = 65\,\text{kW}$ (dashed) at $\alpha_1 = 400\,\text{W/(m}^2\text{K)}$ (curves 1–3); for a linear dependence $\alpha_1(z)$ (curves 4, 5) and various ways of representation of the thermal conductivity coefficient in the solid phase domain. 1: $\lambda_S = 54{\cdot}1\,\text{W/(mK)}$; 2: $\lambda_S = 66{\cdot}2\,\text{W/(mK)}$; 3: $\lambda_S = \lambda_S(T)$; 4: $\lambda_S = \lambda_S(T), \alpha_1(0) = 300, \alpha_1(l) = 500\,\text{W/(m}^2\text{K)}$; 5: $\lambda_S = \lambda_S(T), \alpha_1(0) = 200, \alpha_1(l) = \text{W/(m}^2\text{K)}$.

calculations for zirconium ($a = 0{\cdot}125\,\text{m}$; $l = 0{\cdot}1\,\text{m}$ $\alpha_1 = 400\,\text{W/(m}^2\text{K)}$; $\alpha_2 = 50\,\text{W/(m}^2\text{K)}$; $v_m = 0{\cdot}005\,\text{m/s}$; $b = 0{\cdot}03\,\text{m}$; $R = 0{\cdot}35\,\text{m}$, λ and C_{VL} from [1]) the pool depth oscillates from 20 to 27,2 mm if the absorbed power is changed from $P = 52{\cdot}5\,\text{kW}$ to $P = 105\,\text{kW}$.

In [1] one obtained experimental results for zirconium melting in an autocrucible of diameter 215 mm for a maximum power of $P_0 = 102\,\text{kW}$ ($P = 0{\cdot}7\,\text{kW}$, $P_0 = 71{\cdot}4\,\text{kW}$). The autocrucible bottom was not cooled. The discharge of the zirconium melt for melting with MEMS was equal to $10{\cdot}7\,\text{kg}$ ($1648{\cdot}7\,\text{cm}^3$) and without MEMS it was equal to $3{\cdot}1\,\text{kg}$ ($477{\cdot}8\,\text{cm}^3$). To compare the results we have performed calculations for the following parameters values:

(1) $a = 0{\cdot}1075\,\text{m}$; $l = 0{\cdot}1\,\text{m}$; $b = 0{\cdot}03\,\text{m}$; $P = 71{\cdot}4\,\text{kW}$; $\alpha_1 = 400\,\text{W/(m}^2\text{K)}$; $\alpha_2 = 50\,\text{W/(m}^2\text{K)}$; $v_m = 0{\cdot}3\,\text{m/s}$; $3\,\text{cm} \leqslant R \leqslant 6\,\text{cm}$;
(2) $a = 0{\cdot}1075\,\text{m}$; $l = 0{\cdot}05\,\text{m}$; $b = 0{\cdot}03\,\text{m}$; $P = 71{\cdot}4\,\text{kW}$; $\alpha_1 = 400\,\text{W/(m}^2\text{K)}$; $\alpha_2 = 50\,\text{W/(m}^2\text{K)}$; $v_m = 0{\cdot}005\,\text{m/s}$; $3\,\text{cm} \leqslant R \leqslant 5{\cdot}25\,\text{cm}$.

In the first example the liquid-pool volume is changed from $919\,\text{cm}^3$ to $1633\,\text{cm}^3$ and in the second it is changed from 206 cm and $464\,\text{cm}^3$.

In [20] it was established that melt overheating over melting temperature did not exceed 100 K for the stirring velocity in a liquid pool of $v_m = 1\,\text{m/s}$. This result agrees well with the

values of the maximum temperature on the pool surface obtained by means of our numerical calculations. For niobium ($a = l = 0{\cdot}14\,\mathrm{m}$; $b = 0{\cdot}03\,\mathrm{m}$; $P = 133\,\mathrm{kW}$; $R = 0{\cdot}065\,\mathrm{m}$) the maximum overheating is equal to 101–102 degrees and for the scan radius $R = 0{\cdot}05\,\mathrm{m}$ one achieves 186 K. For zirconium ($a = 0{\cdot}1075\,\mathrm{m}$, $l = 0{\cdot}11\,\mathrm{m}$; $b = 0{\cdot}03\,\mathrm{m}$; $P = 71{\cdot}4\,\mathrm{kW}$) the maximum overheating ranges from 134 K ($R = 0{\cdot}045\,\mathrm{m}$) to 95 K ($R = 0{\cdot}055\,\mathrm{m}$).

8. Conclusions

Comparison of the obtained results with experimental data has shown that the proposed mathematical models correspond adequately to the thermophysical model of the EBAM in a cylindrical autocrucible during axisymmetric heating. Going from the mathematical model to the numerical scheme involves analytical methods. These eliminate the necessity of the approximation of the derivatives with respect to the space variables which is required by the finite-difference method. We have avoid certain undesirable aspects of the finite-element, such as considerable technical difficulties and insufficient economy of the computations.

Applying the Green-function method we were confronted with the necessity of using a constant value of λ_S on the cooled surfaces of the autocrucible. Otherwise the Green function of the Neumann problem which we obtained for the function $u(r, z)$ would not have existed. But we have overcome this obstacle by introducing an auxiliary Green function. This function we constructed applying an equivalent transformation of some of the boundary conditions of the problem.

Regarding future research we must note that the development and investigation of the nonstationary mathematical model is complicated considerably in the case of heating by a scanning electron beam. We can not be certain yet that the corresponding nonstationary Stefan problem will be axisymmetric.

References

1. S. V. Ladokhin and Yu. V. Kornuishin, *Electron-beam Autocrucible Melting of Metals and Alloys*. Kyiv: Naukova Dumka (1988). (In Russian).
2. J. K. Tien and V. C. Nardone, The US superalloy industry – status and outlook. *J. Metals* 9 (1984) 52–57.
3. A. A. Berezovsky and V. D. Dovbnia, Mathematical models of thermal processes in autocrucible during electron-beam autocrucible melting. In: Yu. A. Mitropolsky (ed.), *Nonlinear Boundary Problems*. Kyiv: Institute of Mathematics (1980) pp. 41–57. (In Russian).
4. Yu. A. Mitropolsky and A. A. Berezovsky, Stefan problems with limited steady state in special electric metallurgy, cryosurgery and sea physics. In: *Mathematical Physics and Nonlinear Mechanics* 7: Kyiv: Naukova Dumka (1987) pp. 50–60. (In Russian).
5. Yu. A. Mitropolsky, A. A. Berezovsky and T. A. Plotnitsky, Free boundary problems for nonlinear evolution equation in problems of metallurgy, medicine, ecology. *Ukrainian Math. J.* 44 (1992) 67–76. (In Russian).
6. Yu. A. Mitropolsky, A. A. Berezovsky and S. A. Berezovsky, *Free Boundary Problems for Nonlinear Evolution Equations in Metallurgy, Medicine and Ecology*. Kyiv: Preprint 94.20 of Institute of Mathematics (1994) 54 pp.
7. A. A. Berezovsky, Yu. V. Zhernovyi and M. T. Saychuk, Mathematical modelling of steady-state thermal regime in an autocrucible during electron-beam autocrucible melting. *Heat Physics of High Temperatures* 34 (1996) 125–133. (In Russian).
8. Yu. A. Mitropolsky, A. A. Berezovsky and Yu. V. Zhernovyi, *Free Boundary Problems and Mathematical Modelling of Electron-Beam Autocrucible Melting*. Kyiv: Preprint 97.11 of Institute of Mathematics (1997) 32 pp.
9. M. Salcudean and Z. Abdullah, On the numerical modelling of heat transfer during solidification process. *Int. J. Num. Methods Engng.* 25 (1988) 445–473.

10. D. A. Tarzia, Una revision sobre problemas de frontera movil y libre para la ecuacion del calor. El problema de Stefan. *Mathem. Notae* 29 (1981/82) 147–241.
11. N. N. Rykalin, I. V. Zuyev and A. A. Uglov, *Bases of Electron-Beam Processing of Materials.* Moscow: Mashinostroyeniye (1978) 240 pp. (In Russian).
12. L. A. Volkhonsky, *Vacuum Arc Furnaces*. Moscow: Energoatomizdat (1985) 232pp. (In Russian).
13. A. A. Uglov, I. Yu. Smurov and A. M. Lashin, Modelling of nonstationary movement of phase boundaries during action of energy fluxes on materials, *Heat Physics of High Temperatures* 27 (1989) 87–93. (In Russian).
14. J. Douglas and T. M. Gallie, on the numerical integration of a parabolic differential equations subject to a moving boundary condition. *Duke Math. J.* 22 (1955) 557–581.
15. R. Bonnerot and P. Jamet, Numerical computation of the free boundary for the two-dimensional Stefan problem by spacetime finite elements. *J. Comp. Phys.* 25 (1977) 163–181.
16. R. Bonnerot and P. Jamet, A conservative finite element method for one-dimensional Stefan problems with appearing and disappearing phases. *J. Comp. Phys.* 41 (1981) 357–388.
17. M. Mori, Numerical solution of the Stefan problem by the finit element method. *Memoirs Num. Anal.* 2 (1975) 35–44.
18. A. N. Zelikman, B. G. Korshunov, A. V. Yeliutin and A. M. Zakharov, *Niobium and Tantalum.*, Moscow: Metallurgy (1990) 296 pp. (In Russian).
19. Yu. V. Zhernovyi and M. T. Saychuk, About the numerical solution of the Stefan problems by means of the Green function method. *Engng. and Phys. J.* 71 (1998) 564–570. (In Russian).
20. Yu. F. Anikin, M. I. Taranov, N. M. Kochegura, S. V. Ladokhin, V. L. Shevtsov, Ye. A. Markovsky and S. P. Smirnov, Influence of electron-beam autocrucible melting on structure and properties of heat stable alloy ChS 70, *Problems of Special Electric Metallurgy* 3 (1993) 40–43. (In Russian).